57

OSCILLATION OF LARGE AIR BUBBLE CLOUD

Y. Y. BAE, H. Y. KIM, and J. K. PARK*
KOREA ATOMIC ENERGY RESEARCH INSTITUTE

150 Deokjin-dong, Yuseong-gu, Daejeon, Korea, 305-353
*e-mail: yybae@kaeri.re.kr

KEYWORDS: Two-phase, Analytical, Hydraulics

ABSTRACT

The behavior of a large air bubble cloud, which is generated by the air discharged from a perforated sparger, is analyzed by solving Rayleigh-Plesset equation, energy equations and energy balance equation. The equations are solved by Runge-Kutta integration and MacCormack finite difference method. Initial conditions such as driving pressure, air volume, and void fraction strongly affect the bubble pressure amplitude and oscillation frequency. The pool temperature has a strong effect on the oscillation frequency and a negligible effect on the pressure amplitude. The polytropic constant during the compression and expansion processes of individual bubbles ranges from 1.0 to 1.4, which may be attributed to the fact that small bubbles oscillated in frequencies different from their resonance. The temperature of the bubble cloud rapidly approaches the ambient temperature, as is expected from the polytropic constants being between 1.0 and 1.4.

Nomenclatures

a	Radius of individual bubble, m
b	Damping constant, kg/s
c	Specific heat, J/kg.K
d	Non-dimensional damping constant
H	Submergence, *m*
k	Thermal conductivity, W/m.K
k_{eff}	Effective thermal conductivity defined in Eq. (8)
k_w	Wave number
m	Mass of air, kg
$\dot{m}$	Mass flow rate, kg/s
N	Number of bubbles in a bubble cloud
p	pressure, Pa
R	Bubble cloud radius, m
$\tilde{R}$	Gas constant
r	Radial coordinate (Eulerian), m
S	Surface tension coefficient, N/m
T	Temperature, K

t	Time, sec
v	Velocity, m/s
V	Volume, m^3
x	Radial coordinate (Lagrangian), m
a	Void fraction,
	Thermal diffusivity, m^2/s
k	Polytropic constant
r	Density, kg/m^3
n	Kinematic viscosity, m^2/s
g	Specific heat ratio
w	Angular frequency, s^{-1}

Subscript, superscript

a	Air
amb	Ambient condition near bubble
b	Condition in side bubble
d	End of air discharge
l	Liquid, water
max	Maximum condition
o	Initial condition
, inf	Condition of far from bubble

INTRODUCTION

The oscillation of an air bubble cloud, which consists of many small size bubbles, has long been the subject of extensive research. The oscillation or collapsing of vapor bubbles has especially been studied in depth, since it is a major cause of cavitation damage to rotating or fast moving machinery and ships. Most research on the bubbles focused on small bubbles. The motion of a single bubble can be analyzed by the Rayleigh-Plesset equation [Rayleigh (1917) and Plesset (1949)] (afterwards RPE) and detailed analysis on thermal and viscous effect on the motion have also been performed by many researchers [Chapman & Plesset (1971), Prospereti (1977), Fanelli et al. (1981), Nigmatulin et al.(1981)].

In a Boiling Water Reactor, during transient and accident conditions, air or air-steam mixture in the dry well discharges into the wet well and a large bubble (or bubble cloud) is generated there. The oscillation of a thus generated air bubble may cause significant damage to the adjacent structures if the oscillation frequency is the same or close to the natural frequency of the structures. In order to avoid this damage various types of sparger have been introduced. The functions of the sparger are to reduce pressure force due to the oscillation of bubble as well as to enhance the condensation of steam.

In the design of a conventional Pressurized Water Reactor, no consideration has been given to these phenomena. Following the recent trend of introducing systems for severe accident in order to comply with ever-growing public safety concern, the Korea Next Generation Reactor (KNGR) adopted an In-containment Refueling Water Storage Tank (IRWST), shown in Fig. 1. During the accident, water, air and steam successively discharge into this tank individually or as a mixture. The discharged air forms a bubble cloud and oscillates.

Relatively little interest has been given to the oscillations of a large air bubble cloud of the order of 1.0 m diameter, which consists of many small bubble of 10 – 20

mm diameters as was shown in ABB-Atom Studsvik test (1975) and the test by Kim et al. (1998). The size of the air bubble in this case is several orders of magnitude larger than the bubble size treated in the cavitation problem. The design of a sparger is usually based on experiments, since the phenomena involved are extremely complex and accordingly the analytical approach is difficult.

In this paper we suggest an analytical approach to predicting the behavior of a large air bubble cloud. We first formulate governing equations based on the RPE and energy balance, corresponding boundary conditions, and discuss their solution procedure. The influence of the heat transfer across the bubble surface on damping will be discussed. The results of analysis will be compared with the ABB-Atom Studsvik test (1975), and the applicability of the formulation suggested here will be discussed. Finally the effect of initial and boundary conditions on the bubble cloud motion will be investigated.

MATHEMATICAL FORMULATION

The ambient fluid is assumed to be incompressible. During discharge the air is assumed to expand isentropically, and from then on follows polytropic process. Also it is assumed that the discharged air disintegrates into many 10 mm radius spherical bubbles distributed in the liquid homogeneously, which form a bubble cloud. The degree of distribution density is materialized in the void fraction. We neglect interaction between the small bubbles and the motion of the liquid in the bubble cloud.

Governing equations

The equations governing the air bubble cloud and individual bubbles are expressed as follows.

$$\frac{p_b \quad p}{\rho_L} = R\frac{d^2R}{dt^2} + \frac{3}{2}\left(\frac{dR}{dt}\right)^2 + \frac{4\eta}{R}\frac{dR}{dt} + \frac{2S}{\rho_L R} \tag{1}$$

$$\frac{dp_b}{dt} = 3(\kappa \quad 1)k\left.\frac{T}{r}\right|_{x=a} \quad \frac{3\kappa p}{a}\frac{da}{dt} \tag{2}$$

$$\frac{T}{t} = \frac{k}{\rho_0 c}\frac{1}{x^2}\frac{}{x}\left(\rho\frac{r^4}{x^2}\frac{T}{x}\right) + \frac{1}{\rho c}\frac{dp_b}{dt} \tag{3}$$

$$\rho = \frac{p_b}{\tilde{R}T} \tag{4}$$

$$\frac{r}{x} = \frac{\rho_0}{\rho}\frac{x^2}{r^2} \tag{5}$$

The boundary conditions for (3) are

$$x = 0 : r = 0 : \frac{T}{x} = 0 \tag{6}$$

$$x = R_i : r = R : T_{gas} = T_{liquid} \tag{7}$$

Boundary conditions are not needed for other equations. The Lagrangian coordinate is introduced for the convenience of presenting results. Coordinate x implies the initial radial distance from the origin of the bubble in the Lagrangian coordinate, whereas r implies radial distance in the Eulerian coordinate. All symbols except those otherwise defined possess usual meanings. Equation (1) is the well-known Reyleigh-Plesset equation, (2) the energy balance in the bubble cloud, and (3) the temperature distribution inside the individual bubble. In the derivation of (2) it is assumed that the pressure inside the bubble responds instantly to the external perturbation and stays in an equilibrium state with the external pressure. This can be justified since the flow speed in the field of consideration is much lower than the speed of sound. In (2) the surface velocity of individual bubbles is determined by the following relation.

$$\frac{da}{dt} = \frac{aR^2}{Na^2}\frac{dR}{dt} \tag{8}$$

Equations (1) and (2) are for the bubble cloud, while (3) is for the individual bubbles. As Nigmatulin (1991) pointed out, at the gas and liquid interface the temperature boundary condition is simply given as liquid temperature, due to the high thermal diffusivity in liquid side. The radius of an individual bubbles, a is updated at every time step by applying polytropic process at that time step, not by integrating (8).

$$\frac{a}{a_0} = \frac{p_{b0}}{p_b}^{1/3k} \tag{9}$$

Void fraction in bubble cloud

The traditional analysis method of bubble oscillation assumes that the bubbles are complete spheres. Experimental results, however, show that the air bubble clouds formed around the sparger with many holes (Fig. 2) were never complete spheres and rather a cluster of small bubbles with a considerable amount of water in it. One of the analysis methods we can take in this circumstance is to treat the air bubble as a complete sphere with a certain value of void fraction. Moody (1986) reported a void fraction of 1/2 - 2/3. However, he did not elaborate the conditions where the bubble cloud was generated.

During an experimental investigation of an optimal sparger, Kim et al. (1998) performed an air discharge test for several types of sparger including an open and perforated pipe. Figs. 2 and 3 are snapshots of the air discharge from the perforated and open pipe, respectively and we can see the difference clearly. The air volume and the size of the main pipe are the same for both cases. Through the perforated pipe the air breaks into many small bubbles and forms a bubble cloud, whereas the air discharged through the open pipe shows no serious disintegration and maintains a spherical shape (above the inclined branch pipes). The videotape of ABB-Atom's test, where the same type of sparger as the one in KNGR was used, shows similar phenomenon of air bubble cloud, but on a large scale. The void fraction was estimated from the snapshots of both cases of perforated pipe and open straight pipe. By comparing the size of the air bubble cloud from the two types, the void fraction was estimated as about 0.2. It is smaller than that suggested by Moody(1986). This may be attributed to the high discharge speed.

Initial conditions

In the case of cavitation, the initial condition is given as the perturbation in the far field. In contrast, in our case the initial condition is usually given by the condition around the nozzle where the discharged air develops into a large air bubble cloud. Solution of (1) is a function of two initial conditions R_0 and dR_0/dt. The initial condition is the state of air after discharge and is a function of the condition upstream of the sparger, which is determined simply by one-dimensional transient pipe flow by Method of Characteristics. For details, please refer to Bae and Kim (1999).

The air in the pipe compressed by steam discharges through the holes of the sparger with sonic speed and quickly expands to the ambient pressure. Then the total mass flow rate through the holes is

$$\dot{m} = (\quad a_{hole}) p_0 \sqrt{\frac{g}{R_{air} T_0} \quad \frac{2}{g+1}^{\frac{g+1}{g\ 1}}} \tag{9}$$

The frictional loss across the holes is neglected. The volume of the bubble cloud is expressed as

$$V(t, t \quad t_d) = \frac{1}{\mathrm{ar}_{a,amb}} \int_0^t \dot{m}\, dt = \frac{\dot{m} t}{\mathrm{r}_{a,amb}} \tag{10}$$

where $t_d = \mathrm{r}_{a,amb} V_o / \dot{m}$ is the time duration of air discharge. The discharged air expands to ambient pressure, and the volume of air bubble cloud is obtained by dividing the discharged air volume by void fraction. The initial conditions of radius and surface speed of the bubble are

$$R(t, \ t \quad t_d) = \frac{3V(t)}{4\mathrm{p}}^{1/3} \tag{11}$$

$$\dot{R}(t, t \quad t_d) = \frac{\dot{m}}{4\mathrm{p}R^2 \mathrm{r}_{a,amb}} \tag{12}$$

During the discharge period, the pressure inside the air bubble cloud is assumed to be that of the ambient condition, which is atmospheric pressure plus hydrostatic pressure.

$$p_b(t, t \quad t_d) = p_{atm} + \mathrm{r}_l g H \tag{13}$$

During the discharge period, an air bubble discharged earlier will be subjected to additional force due to the reflected wave in the driving steam in the piping and also it will undergo oscillation. Also there exist two or three pressure peaks during the discharge period as a result of initial discharge through load reduction ring and sparger in series. We will not go into detail since this is beyond our discussion and has a negligible effect on subsequent oscillation after full discharge. According to Bae and Kim (1999), the air discharge period is extremely short, less than 200 ms

when the pressure of driving steam is 10 bar. Since the temperature of the air after isentropic compression and the expansion process is just the same as the initial condition, we set the initial temperature boundary condition as

$$T_b(t, t \quad t_d) = T_{amb} \tag{14}$$

Here the energy loss during the discharge process is neglected.

Damping

There are three types of damping for the oscillation of bubble such as thermal, viscous and radiation. As is shown in Fig. 4, when the bubble is small and (order of millimeters or even smaller) at resonance, the viscosity is a dominant factor of damping. As the bubble size increases, viscose damping decreases rapidly, and thermal and radiation damping gradually become controlling factors. The frequency of bubble cloud oscillation is much lower than that of the individual.

Therefore, individual bubbles experience the off-resonance oscillation [Brennen (1995)]. The damping constants at resonance given in Fig. 4 [Leighton (1994)] are completely different from those at off-resonance. The non-dimensional damping constants at off-resonance oscillation are given as follows [Eller (1970)].

$$\begin{aligned} d_{th} &= \mathrm{w}b_{th} / k_{\mathrm{w}} \\ &= 3(\mathrm{g} \quad 1)\, \frac{X(\sinh X + \sin) \quad 2(\cosh X \quad \cos X)}{x^2(\cosh X \quad \cos X) + 3((\mathrm{g} \quad 1)X(\sinh X \quad \sin X)} \end{aligned} \tag{15}$$

$$d_{rad} = \mathrm{w}b_{rad} / k_{\mathrm{w}} = \mathrm{r}_l a_0^3 \mathrm{w}^3 / 3\mathrm{h}p_0 c \tag{16}$$

$$d_{vis} = \mathrm{w}b_{vis} / k_{\mathrm{w}} = 4\mathrm{w}\mathrm{m} / 3\mathrm{h}p_0 \tag{17}$$

where

$$k_{\mathrm{w}} = 3\mathrm{h}p_0 / 4\mathrm{p}a_0^3 \tag{18}$$

$$\mathrm{h} = \mathrm{g}(1 + d_{th}^2)^{\ 1}\ 1 + \frac{3(\mathrm{g} \quad 1)}{X}\frac{\sinh X \quad \sin X}{\cosh X \quad \cos X}^{\ 1} \tag{19}$$

$$X = a_0(2\mathrm{w}/\mathrm{a})^{1/2} \tag{20}$$

The term X means the ratio between bubble radius and the thermal penetration depth. The dimensional damping constant b is defined in the equation of motion of bubble

$$m\ddot{v} + b\dot{v} + k_{\mathrm{w}} v + p_A e^{j\mathrm{w}t} = 0 \tag{21}$$

We will not use this equation and it is introduced just to show how the effective thermal conduction coefficient is materialized. The non-dimensional damping constants given by (15) - (17) are shown in Fig 5. When the oscillation frequency of

bubble cloud is 10 Hz, which is order of oscillation frequency of 0.5 m radius bubble cloud, for the individual bubble of 10 mm radius the thermal damping is dominant over the radiation and viscous damping. We thus neglect the viscous and radiation damping afterwards.

Solution procedures

Governing equations (1) - (5) are solved with boundary conditions (7) and (8) and initial conditions (11) - (14) numerically. The grid is generated by the following simple equation. The number of grid N is chosen so that a sufficient number of grids are in the thermal boundary layer.

$$R_j = jR/N, \quad j = 0,1,2,3...,N \qquad (22)$$

This simple equal spaced grid with $N = 10$ was sufficient to cover the thermal boundary layer, since the layer was the same order of radius of the bubble. Equation (3) is integrated by the MacCormack predictor-corrector method and the other equations are integrated by the fourth-order Runge-Kutta method. The time step is chosen so that the stability criterion $S = \mathrm{a}\ t/(\ x)^2 \quad 0.5$ is not violated.

OSCILLATION FREQUENCY

In ABB-Atom test at Studsvik (1975) the air is discharged into a tank of 1.5 m diameter and 5.0 m high. The recorded frequency of the air bubble cloud in the Studsvik test was about 5 Hz (initial air volume is 0.496 m^3 in ATP), while the frequency from the analysis by RPE without consideration of heat transfer is about 8 Hz (based on the hydrostatic pressure around the bubble cloud 1.45 x 10^5 Pa). The difference may be attributed to the thermal damping and two dimensional effect.

RESULTS AND DISCUSSION

The pressure on the wall due to the bubble oscillation is expressed as [Moody (1990)]

$$P(\ ,t) \quad P = \frac{2R}{\sqrt{D^2 + \ ^2}}\ (p_b \quad p\ ) + \frac{\mathrm{r}}{2g_0}\ \frac{dR}{dt}^2 \div 1\ \frac{2R^3\ ^2}{\left(D^2 + \ ^2\right)^{5/2}} \qquad = \sqrt{y\ + z^2} \quad (23)$$

where D and are the horizontal and vertical distances from the bubble cloud to the point at the wall. In our case the dynamic pressure term is negligible. Maximum wall pressure occurs when $= 0$. The radius of bubble cloud, 0.8 m, is nearly half of the radius of the tank, 1.5 m. This means that the wall pressure is nearly the same as the bubble pressure, and it allow us to compare the wall pressure measured by the Studsvik test with calculated results directly. In Fig. 6 pressure history inside the bubble during oscillation is shown. The solid line shows the result of the numerical simulation, while the symbols represent the ABB-Atom test results. Due to the initial radial velocity, the bubble cloud expands first to maximum radius beyond equilibrium radius (corresponding to minimum pressure), then compresses to minimum radius (corresponding to maximum pressure) and oscillates subsequently. The two initial peaks come from the initial discharge from the load reduction ring and sparger, respectively. Since the load reduction ring is located upstream of the sparger by a certain distance the compressed air discharges first through the load reduction ring,

and with a certain time lag discharges through the sparger. This serial discharge with time lag is believed to reduce the peak pressure, if not confirmed analytically. Figures. 7 and 8 show the histories of the radius and surface speed of the bubble cloud.

The effect of driving steam pressure on pressure history is shown in Figure. 9. The amplitude increases as the driving pressure increases. The frequency does not change as the driving pressure changes.

Figure 10 shows the effect of initial air mass on the pressure history. As the air mass increases the amplitude decreases. Arinobu et al. (1983) reported a similar case. In that report the authors presented a graph (Fig. 3 of referenced paper), which shows that the bubble peak pressure increases as the bubble radius (may be interpreted as initial air mass in our case) increases. This is somewhat misleading. In their report, the initial bubble surface velocity is fixed and the size of the bubble varies independently. Accordingly, the bubble peak pressure increases as bubble size increases. However here the initial bubble surface velocity is inversely proportional to the square of the bubble radius, and the bubble peak pressure decreases as the initial air mass increases if the driving pressure is fixed. Contrary to Figure 9, the air mass has a significant effect on the oscillation frequency as well as amplitude. The large air mass means that when the void fraction is fixed, a large diameter of bubble cloud results in a large volume of water to be displaced. This may be the reason for the decrease of oscillation frequency as air mass increases.

The influence of pool temperature on bubble pressure is shown in Figure 11. Contrary to the driving pressure, pool temperature affects the frequency more than bubble pressure. This result is not consistent with the ABB-Atom's test, wh ere the pressure is reported as a strong function of pool temperature. The strong dependence of bubble pressure on pool temperature may be related to the presence of steam in the bubble cloud and its interaction with pool water, which we do not consider here. The steam content of the air bubble cloud will considerably affect its motion through condensation, since steam condensation is a very violent phenomenon and the condensation heat transfer coefficient is several orders of magnitude larger than conventional heat transfer by convection and conduction.

The effect of the void fraction shown in Figure 12 may be interpreted in the same way as was done for the air mass. The higher value of the void fraction with fixed air mass means larger bubble cloud size and will result in a lower peak. The effect of the void fraction looks very significant. The bubble cloud volume of $a=0.5$ is 5 times larger than that of $a=0.1$. This explains the very large pressure amplitude for $a=0.5$. Also as we saw in the case of air mass, the void fraction affects the frequency significantly.

Prosperetti (1977) reported that the polytropic constant approaches the isothermal limit, $k=1$, as the square of the ratio between the bubble radius and the thermal penetration depth decreases, while it approaches to isentropic limit, $k=1.4$, as the ratio increases to a certain limit, afterwards it rapidly falls down to a value below the isothermal limit. Crum (1983) experimentally investigated the thermal behavior of a gas-air mixture bubble and compared it with analytical results. His results confirm the trend of a polytropic constant as reported by Prosperetti (1977). Instantaneous polytropic constant calculated by $k = d(\ln p)/d(\ln r)$ is shown in Figure 13. The polytropic constant ranges from 1.0 to 1.40, leaned a little bit to 1.4, if not significantly. The trend of the polytropic constant change is different from that of Bae et al. (2000) and Nigamtulin (1991). This may be attributed to the fact that the individual bubbles in the bubble cloud oscillate in the frequency of the bubble cloud, which is very different from that at resonance. This gives sufficient time for heat

diffusion into the interior of the individual bubble, which is clearly seen in *Figure 15*. Whenever the bubble cloud reaches minimum or maximum radius, the polytropic constant changes from 1.0 to 1.4, that is, isothermal limit to isentropic limit, and during the period in-between the constant decreases monotonically from 1.4 to 1.0. The bubble undergoes a lower frequency than it will do at resonance. The reader should not be confused with the scattered points beyond or below the two reference lines of $k=1.0$ and $k=1.4$. Those deviations are from errors in numerical integration.

Figure 14 shows the effect of ambient temperature on the average temperature in the individual bubbles in cloud. As the oscillation proceeds, the average temperature approaches the ambient temperature very rapidly. As we have seen when we discussed the polytropic constant the thermal boundary is very thick and most of the region inside the bubble is within the range of influence of heat exchange across the surface.

As we discussed, when we analyze the polytropic constant, the thermal boundary layer on the individual bubble surface is significantly thick. It is clearly seen in Figure 15, which shows the evolution of radial temperature distribution during one cycle of oscillation from the first maximum to the second maximum of the radius. Heat transfer through the bubble surface is felt by the thick thermal boundary layer. The time $t=0$ implies maximum radius or minimum pressure. At $t=0$, the temperature of the majority of the bubble is at a minimum due to maximum expansion. As the bubble expands it is first felt by the gas in the region near the boundary, and the temperature there rises faster than the other regions. This is clearly shown at $t=\pi/2$. At this point, although the temperature of the majority of the bubble is lower than the pool temperature, the heat transfer is directed from the gas to the pool water. At around $t=7\pi/4$ the reversed phenomenon occurs, that is, the temperature of the majority of the bubble is higher than the pool temperature and the heat transfer is directed from the pool water to the gas.

CONCLUSIONS

The behavior of a large bubble cloud of 1 m diameter, which consists of many 20 mm diameter air bubbles and with water in it, was investigated. The governing equations based on Rayleigh-Plesset equation modified by the inclusion of an energy equation are solved by Runge-Kutta integration and MacCormack's predictor-corrector finite difference scheme. From the analysis the following conclusions were obtained.

1) The suggested method of analysis reproduced the ABB-Atom test results reasonably and the applicability of the method is confirmed.
2) As driving pressure increases, pressure amplitude increases
3) As initial air mass increases, pressure amplitude decreases.
4) The ambient temperature has an effect on the pressure amplitude, but the degree is rather small.
5) The void fraction has a significant effect on both the amplitude and frequency. Accurate estimation of this may be the key to correct analysis of the bubble cloud.
6) The polytropic constant in the compression and expansion process of individual small bubbles ranges from 1.0 to 1.4, which may be attributed to the fact that small bubbles oscillate in frequencies different from their resonance.
7) The temperature of the bubble cloud rapidly approaches the ambient temperature, as is expected from the polytropic constants.

ACKNOWLEDGEMENT

This research has been performed as a part of the long-term nuclear energy development program supported by Ministry of Science and Technology of Korea.

REFERENCES

ABB-Atom Studsvik safety relief valve discharge test (1974-1975), 1975, ABB-Atom.

Arinobu, M., Shioyama, T. and Shiho, E., 1983, "Evaluation of Dynamic Loads Due to Bubble Oscillation Caused by S/RV Actuation," Transaction of the 7th International Conference on Structural Mechanics in Reactor Technology, North-Holland, pp. 67-74.

Bae, Y. Y., Kim, H. Y., Chang, M. H., and Park, J. K., 2000, "A Study of the Air Discharge and Subsequent Oscillation with Heat Transfer," ASME 2000 Fluids Engineering Division Summer Meeting, FEDSM 2000, Boston, MA, June 11-15, 2000.

Bae Y. Y., and Kim, H. Y., 1999, "Numerical Simulation of Unsteady Flow Through Pipe Including Sparger with Load Reduction Ring," Proceedings of 3rd ASME/JSME Joint Fluid Engineering Conference, July 18-23, San Francisco.

Brennen, C. E., 1995, *Cavitation and Bubble Dynamics*, Oxford University Press.

Chapman, R. B. and Plesset, M. S., 1971, "Thermal effects in the free oscillation of gas bubbles," J. of basic Engineering, September, pp. 373-376.

Crum, L. A., 1983, "The polytropic exponent of gas contained within air bubbles pulsating in a liquid," J. Acoust. Soc. Am. Vol. 73(1), pp. 116-120.

Eller, A. I., 1970, "Damping constants of pulsating bubbles," J. Acoust. Soc. Am. Vol. 47, No. 5 (paret 2), pp. 1469-1470.

Fanelli, M., Properetti, A., and Reali, M., 1981, "Radial Oscillations of gas bubbles in liquids Part I: Mathematical formulations," Acustica, Vol. 47 (4), pp. 253-265.

Kim et al., 1998, "A Study on the Behavior of Bubble in Quenching Tank and Optimal Sparger Design," KAERI/TR-962/98, (in Korean).

Leighton, T. G., 1994, *The Acoustic Bubble*, Academic Press.

Moody, F. J., 1986, "Dynamics and Thermal Behavior of Hot Gas Bubbles Discharged into Water," Nuclear Engineering and Design, Vol. 95.

Nigmatulin, R. I., Khabeev, N. S., and Nagiev, F. B., 1981, "Dynamics, Heat and Mass Transfer of Vapor-Gas Bubbles in a Liquid," Int. J. Heat Mass Transfer, vol. 24, No. 6, pp. 1033-1044.

Nigmatulin, R. I., *Dynamics of Multiphase Media*, Volume 1, 1991, Hemisphere Publishing Corporation,

Prosperetti, A., 1977, "Thermal effects and damping mechanisms in the forced radial oscillations of gas in liquids," J. Acoust. Soc. Am. Vol. 61 (1), pp. 17-27.

Plesset, M. S., 1949, "The dynamics of cavitation bubbles," ASME J. Appl. Mech. Vol. 16, pp. 228-231.

Rayleigh, Lord, 1917, "On the pressure developed in a liquid during the collapse of a spherical cavity," Phil. Mag. Vol. 34, pp. 94-98

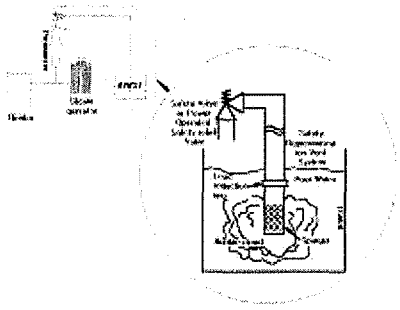

Fig. 1 Schematic drawing of safety depressurization system.

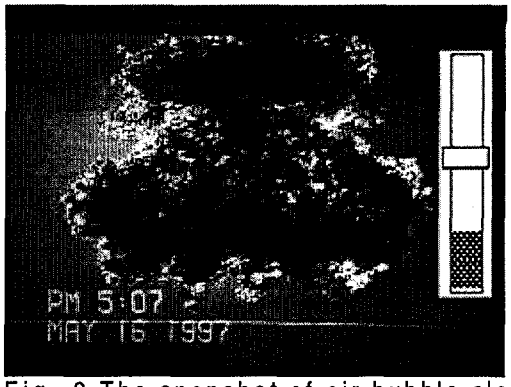

Fig. 2 The snapshot of air bubble cloud discharged from a perforated sparger.

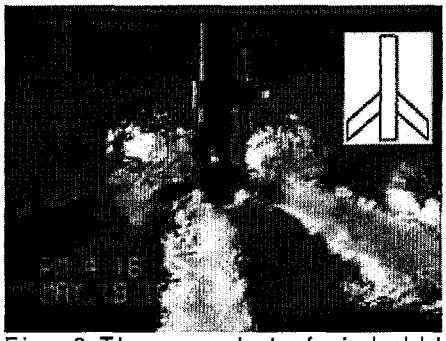

Fig. 3 The snapshot of air bubble cloud discharg ed from a three prong straight sparger.

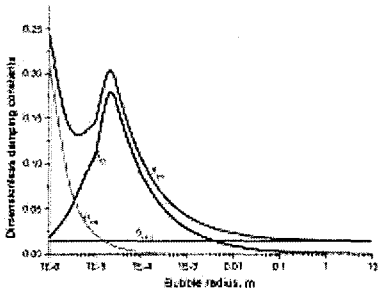

Fig. 4 Damping constant at resonance.

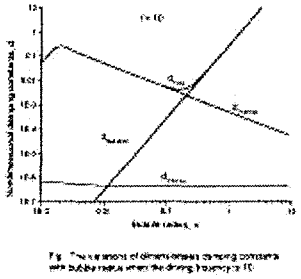

Fig. 5 Damping constant at off -resonance versus bubble radius, when f=10.

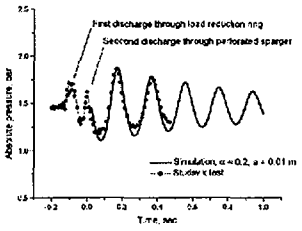

Fig. 6 Comparison of numerical simulation with test results.

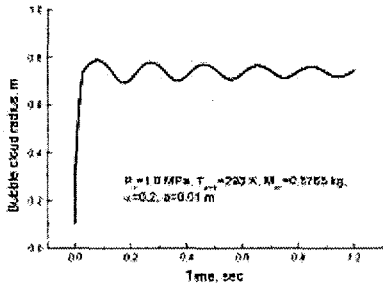

Fig. 7 Bubble radius versus time.

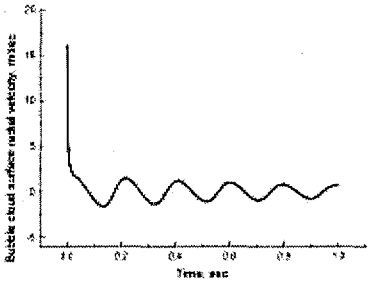

Fig. 8 Bubble surface velocity versus time.

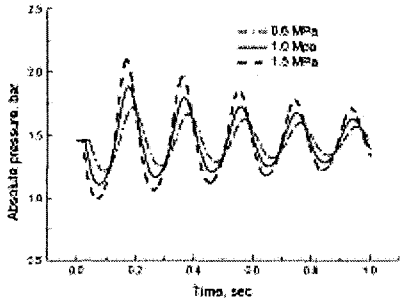

Fig. 9 The effect of driving steam pressur e on the bubble pressure history.

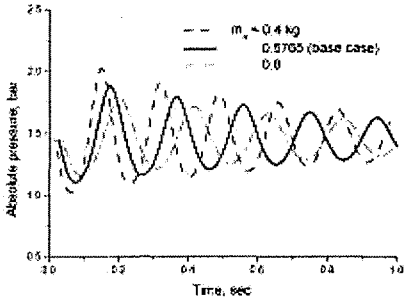

Fig. 10 The effect of initial air mass on the bubble pressure history.

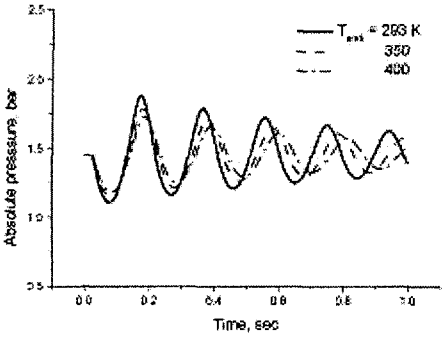

Fig. 11 The effect of ambient temperature on the bubble pressure history.

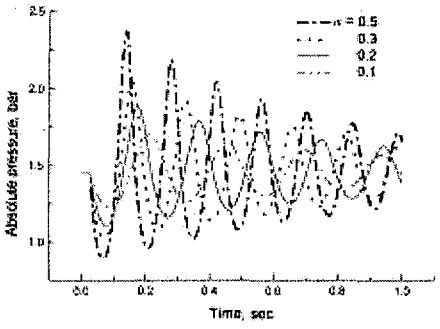

Fig. 12 The effect of void fraction on the bubble pressure history.

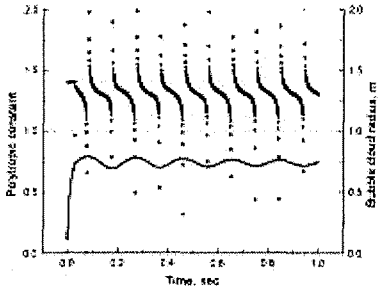

Fig. 13 Evolution of polytropic constant during the oscillation of bubble cloud.

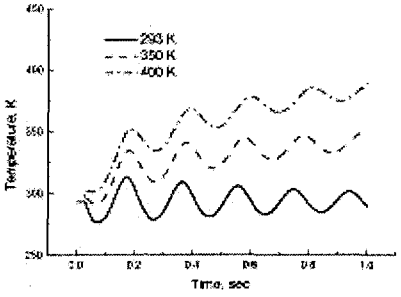

Fig. 14 The effect of ambient temperature on the averag e temperature inside bubble.

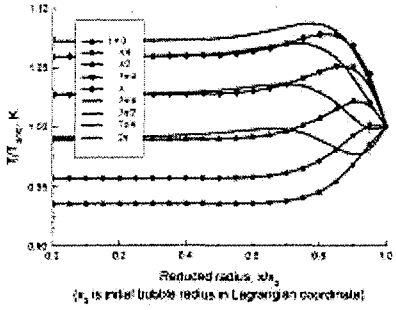

Fig. 15 Evolution of temperature distribution inside bubble.